Journal of Molecular Structure (Theochem), 200 (1989) 443–462
Elsevier Science Publishers B.V., Amsterdam — Printed in The Netherlands

THE VIBRATIONAL SPECTRA, MOLECULAR STRUCTURE AND CONFORMATION OF ORGANIC AZIDES
Part XI. An ab initio, IR matrix isolation and Raman temperature study of 3-azidopropene (allylazide)*

ANTON GATIAL**, PETER KLAEBOE, CLAUS JØRGEN NIELSEN*** and HANNO PRIEBE†

Department of Chemistry, University of Oslo, P.O. Box 1033 Blindern, N-0315 Oslo 3 (Norway)

(Received 8 May 1989)

ABSTRACT

3-Azidopropene, $CH_2=CH-CH_2-N_3$, has been synthesized by a safe, small-scale procedure applicable also to other azides. IR spectra have been recorded of the liquid, the amorphous solid, and the matrix isolated species in N_2 and Ar at 14 K. Raman spectra of the liquid at different temperatures and of the amorphous and crystalline solids were also obtained.

Fully optimized geometries for the five distinct conformations of 3-azidopropene have been calculated at the SCF level employing a basis set of double zeta quality and compared with the recent results from electron diffraction. The calculations show that the GG conformation is the most stable, followed, in decreasing order of stability, by SG (+2.1 kJ mol^{-1}), SA (+5.3 kJ mol^{-1}), GG′ (+6.4 kJ mol^{-1}) and GA (+6.5 kJ mol^{-1}), where the capital letters refer to the conformation around the C–C and C–N bonds respectively.

The IR and Raman spectral data show the GG to be the most stable conformer both in the N_2 and Ar matrices, as well as in the liquid. Whereas the low-temperature crystalline solid is made up of molecules in the SG conformation. Apparently, all five conformers are observed in the liquid at room temperature and trapped in the Ar matrix at 14 K, whereas only three conformers (GG, SG and GG′) were observed in the N_2 matrix.

In the liquid phase the enthalpy difference between the GG and SG conformations was found to be $\Delta H^{\circ}_{GG\rightarrow SG} = 1.3(3)$ kJ mol^{-1}. The corresponding results for the SA and GA conformations were 5.2(22) and 4.4(7) kJ mol^{-1} respectively, and $\Delta H^{\circ}_{GG\rightarrow GG'}$ was estimated as 3.5 kJ mol^{-1}.

INTRODUCTION

3-Azidopropene ($CH_2=CH-CH_2-N_3$, allylazide, ALAZ) can exist in five dis-

*Part X of this series is given as ref. 1.
**On leave from Department of Physical Chemistry, Slovak Technical University, Bratislava, Czechoslovakia.
***Author to whom correspondence should be addressed.
†Present address: NYCOMED, P.O. Box 4220 Torshov, N-0401 Oslo 1, Norway.

0166-1280/89/$03.50

tinct conformations, labeled SA, SG, GA, GG and GG′ respectively, and depicted in Fig. 1. We have recently reported the results from a study of ALAZ by vibrational spectroscopy and electron diffraction [2], where it was concluded that ALAZ exists in the vapour phase as (1) a mixture of two conformers, 73(15)% GG and 27% SG, or (2) a mixture of equal amounts of the GG and GG′ forms, 87(20)% in total, and 13% SG, or (3) a linear combination of these two cases. The other two conformers, SA and GA, were estimated to be present at less than 5% in the vapour phase at 300 K. The vibrational spectra [2] were interpreted in terms of the GG and SG conformers being present in the vapour and liquid and the SG conformer being present in the crystalline solid. This interpretation was partly based upon normal coordinate calculations, using transferred scaled quantum mechanical force fields from azidoethane [3] and propene [4], and partly upon preliminary results from the present ab initio calculations.

The ambiguous results for the conformational composition, and the unusual situation in which the conformer present in the crystal is not the most stable in the liquid (and in the vapour), led us to extend our studies on ALAZ by ab initio calculations, IR matrix isolation and Raman studies of the solid and of the liquid at different temperatures. The present work also constitutes an extension to our more general ab initio studies of organic azides [5,6].

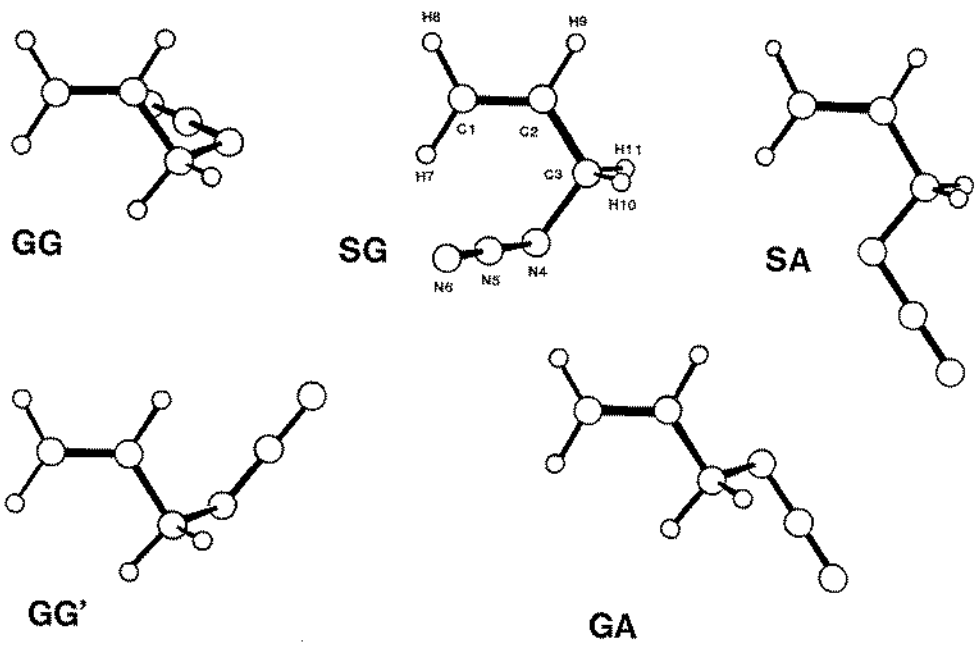

Fig. 1. The five possible conformations of 3-azidopropene. SA: $\tau_{C\text{-}C}=0°$, $\tau_{C\text{-}N}=180°$; SG: $\tau_{C\text{-}C}=0°$, $\tau_{C\text{-}N}\approx 60°$; GA: $\tau_{C\text{-}C}\approx 0°$, $\tau_{C\text{-}N}=180°$; GG: $\tau_{C\text{-}C}\approx 120°$, $\tau_{C\text{-}N}\approx 60°$; GG′: $\tau_{C\text{-}C}\approx 120°$, $\tau_{C\text{-}N}\approx -60°$.

EXPERIMENTAL

Preparation

Tetramethylguanidinium azide (ca. 15 g, 90 mmol) was dissolved in sulfolane (100 ml) and the solution degassed at 50 °C for 4 h in vacuum. 3-Bromopropene (ca. 3 ml, 4 g, 45 mmol) dissolved in sulfolan (20 ml) was added to the solution at 50 °C. After 2 h the product was sucked into a trap, cooled with liquid N_2, recondensed and dried by vacuum distillation through a U-shaped tube, which was partly filled with phosphorus pentoxide.

The method outlined above has also been used to prepare several more "dangerous" organic azides in our laboratory and it appears to be quite safe in small-scale synthetic work.

Spectra

IR matrix isolation spectra were recorded with a Perkin–Elmer model 225 spectrometer using a closed-cycle He-cooled cryostat from Air Products. Spectra were obtained with both N_2 and Ar as matrix materials at matrix/absorber-ratios between 1:500 and 1:1000. The gas mixtures were passed through an electrically heated quartz nozzle [7] before being deposited on the cold CsI window kept at 14 K. No pyrolysis products were detected at the nozzle temperatures employed: 300 and 600 K for the N_2 and 300, 450, 600 and 650 K for the Ar matrix experiments. The matrices were annealed for 15–30 min at temperatures in the range 24–35 K and ultimately up to 12 h at 35 K.

The Raman spectra were recorded with a DILOR RTI30 spectrometer (triple monochromator) interfaced to the Aspect 2000 data system of a Bruker FTIR. The 514.8-nm line of a Spectra Physics Model 2000 Ar^+ laser was used for excitation. Spectra of the liquid were obtained in the temperature range 148–260 K. The liquid was sealed in a capillary tube of 2-mm inner diameter inserted into a transparent Dewar [8] and cooled by a stream of N_2 evaporating from a reservoir equipped with a heating element. The temperature was measured by a thermocouple situated close to the scattering point and checked by carefully measuring the low-frequency anti-Stokes and Stokes lines. The liquid gradually turned glassy with decreasing temperature, but appeared stable for hours in the laser beam. However, as a safety precaution, the laser power was kept below 150 mW at the sample, as violent explosions of azides have previously occurred in the laser beam.

Attempts to crystallize the sample in conventional cryostats were unsuccessful: a crystalline sample could not be obtained on the mid-IR or far-IR cryostats. The sample turned solid at 108 K and sometimes cracked and looked apparently crystalline. However, the spectra show that the solid sample obtained this way is amorphous. It was possible to reproduce the experiment

reported previously [2], in which the sample was annealed in a capillary, placed just above the surface of liquid nitrogen for 2 days. This sample was kept crystalline in the transparent Raman Dewar or immersed in liquid N_2 for 2 weeks and several Raman spectra were recorded, also in the anti-Stokes region. The sample was allowed to melt partly while being monitored by the Raman scattering, and when cooled again below the melting point, 135 K, it crystallized perfectly. When the sample was allowed to melt completely it was not possible to obtain the crystal again simply by cooling.

COMPUTATIONAL DETAILS

Equilibrium structures of the different conformations of ALAZ were calculated on the Hartree–Fock level, using a gradient version of the program MOLECULE [9,10]. The geometry relaxation was continued until all cartesian forces at the atoms were less than 0.001 a.u. The primitive basis sets employed, *7s3p* for C and N [11] and *4s* for H [12], were contracted to double zeta quality (*4s2p* on C and N, *2s* for H), the orbital exponents on hydrogen being scaled by 1.44 [13].

RESULTS

Ab initio calculations

The five conformational energies which result from the geometry relaxation are given in Table 1, which also shows estimates of the abundance of each conformer at 150, 300 and 600 K respectively. The computed equilibrium geometries of the conformers are compared with the experimental results from electron diffraction ($r_a \angle_\alpha$) [2] in Table 2. The gross atomic charge distribution of the azide group is computed as $q_{N4} = -0.28$, $q_{N5} = -0.07$ and $q_{N6} = 0.05$. Naturally, the individual components of the dipole moment vector vary sig-

TABLE 1

Ab initio calculated energies and the estimated abundance of the five distinct conformations of 3-azidopropene at different temperatures (see Fig. 1)

Conformation	Energy (hartree)	ΔE (kJ mol^{-1})	Abundance (%)		
			150 K	300 K	600 K
SA	−279.359825	5.3	0.6	3.7	7.3
SG	−279.361021	2.1	15.4	26.1	27.5
GA	−279.359358	6.5	0.5	4.5	11.5
GG	−279.361826	0	83.0	60.9	42.0
GG′	−279.359405	6.4	0.5	4.8	11.7

TABLE 2

Ab initio calculated structures (pm, deg.) of the five conformations (SA, SG, GA, GG and GG′; see Fig. 1) of 3-azidopropene compared with the results from electron diffraction

Parameter	SA	SG	GA	GG	GG′	Experimental
Distances						
C1=C2	131.3	131.4	131.4	131.5	131.4	133.1(7)
C2–C3	150.0	150.8	149.7	150.1	150.2	150.8[b]
C3–N4	150.2	150.4	151.3	151.5	151.5	147.5(15)
N4=N5	125.1	126.0	125.5	125.8	125.5	123.6(5)
N5=N6	111.3	111.1	111.3	111.1	111.3	113.8(4)
C1–H7	106.8	107.0	107.2	107.3	107.2	
C1–H8	107.1	107.0	107.0	107.0	107.0	
C2–H9	107.3	107.4	107.1	107.2	107.4	109.4(15)
C3–H10	108.4	108.3	108.1	108.2	107.5	
C3–H11	108.4	107.7	108.4	107.5	108.2	
Angles						
C2=C1–H7	121.7	121.8	122.2	122.0	122.0	
C2=C1–H8	120.9	121.3	121.6	121.8	121.7	120.8[b]
C1=C2–H9	120.3	120.1	120.9	120.4	119.8	
C1=C2–C3	125.7	125.4	124.2	124.1	124.1	121.6(30)[c]
C2–C3–N4	108.8	113.8	106.5	111.8	112.3	111.8(34)[c]
C2–C3–H10	109.9	110.2	111.1	111.2	111.2	
C2–C3–H11	109.9	110.4	110.5	111.4	111.1	109.0[b]
N4–C3–H10	110.4	110.9	110.6	110.9	103.5	
N4–C3–H11	110.4	103.8	109.9	102.8	110.0	
C3–N4=N5	114.2	113.3	113.6	113.1	113.5	115.1(14)
N4=N5=N6	173.3	173.2	173.3	173.6	173.3	174(5)
Torsional angles						
C3–C2=C1–H7	0	0.4	1.9	0.6	0.5	0[b]
C3–C2=C1–H8	180	179.4	−178.4	−179.6	−179.6	180[b]
C3···C1=C2–H9	180	−179.2	179.2	178.9	179.7	180[b]
C1=C2–C3–N4	0	10.1	−130.3	121.9	−117.6	120[b,d]
C2–C3–N4=N5	180	79.4	−172.1	−65.1	−71.0	60(10)
C3–N4=N5=N6	180	179.0	−179.2	179.8	−178.8	180[b]

[a]Electron diffraction data (r_a, $\angle_\alpha$) from ref. 2. [b]Assumed. [c]The corresponding angle in the SG conformer was constrained to be 1.5° larger. [d]The corresponding torsional angle in the SG conformer was constrained to 0°.

nificantly from conformer to conformer. However, the computed dipole moments are all ca. 2.1 D (7.0×10^{-30} C m) directed along the C–N bond within 10°, the azide group being the negatively charged end. For comparison, the experimental value obtained from a benzene solution is 1.92 D [14].

TABLE 3

Infrared and Raman spectral data[a] for 3-azidopropene (allylazide)

Infrared						Raman			Interpretation
Ar matrix		N_2 matrix		Solution 300 K	Amorphous solid 80 K	Liquid 260 K	Amorphous solid 80 K	Crystalline solid 80 K	
600 K[b]	Ann.	600 K	Ann.						
3101 w[c]		3097 w		3090 s	3085 m	3090 m	3088 m	3089 m	ν_1
3090 vw,sh	*				~3080 mw,sh				
3082 vw		3081 vw		3070 m	3069 w			3071 w	
3044 vw		3037 vw							
3020 vw		3021 vw		3020 m	3016 mw	3020 vs	3018 vs	3018 s	ν_2
2998 w		2998 w		2989 s	2985 m	2989 s	2984 s	2991 w	ν_3
2994 vw	*	2994 vw	*						
2971 w		2973 w		~2970 m,sh	~2975 w,sh	~2975 vw,sh		2960 m	ν_4
2966 vw	*								
2944 w		2940 vw							
2933 vw	*	2935 w,bd	⇑	2925 s	2932 s	2932 m	2936 m	2926 m	ν_5
2925 w		2926 vw,sh	⇓		~2920 vw,sh	2917 m	2915 w	2913 w	
				~2910 m,sh	~2910 w,sh				
2886 w,bd	⇓	2886 w	⇑						
2881 w,sh	⇑	2881 vw,sh	⇓	2875 m	2879 m	2880 mw	2880 w	*	
2872 vw	⇓	2875 vw,sh	⇓	~2860 m,sh		2860 vw,sh	~2860 vw,sh	2866 w	
		2139 m,sh	⇓						
2135 s		2134 s			~2150 s,sh				
2124 s	*	2127 s,sh	⇓		2125 vs,sh		~2125 vw,sh		
2113 vs		2113 vs		2105 vs	2103 vs	2104 w	2105 w	2097 m	ν_6
2106 s,sh									
2099 s,sh	*	2102 m,sh	*						
2096 s,sh	*	2095 m	⇓						
2080 vs		2079 vs		2080 s,sh	2074 vs,sh	2076 w	2073 w	2066 w	
2053 vw		2055 vw			2048 w,sh				
1654 vw,+	*			1651 w,sh	1647 w,sh	1646 s,sh,+	1647 s,sh	1648 m	ν_7 (SG)
					1644 m,sh				

1648 w	⇑	1648 w		1645 m,sh	1642 m	1642 vs	1641 vs	*	ν_7 (GG)
1642 vw,+	*	1642 vw		1642 m,sh	1638 w,sh				ν_7(GG′)?
				1634 w,sh	1635 w,sh				
						1618 vvw	~1616 vw		
1464 vw	*	1463 vw,sh	*		~1465 vw,sh				
1458 mw	⇑	1458 mw	⇑		1458 mw,sh				
1453 vw,sh	⇑	1456 w,sh	⇓	1452 m	1453 m	1455 w	1453 w	*	ν_8(GG)
1449 vw	*	1452 vw,sh	*		1448 mw,sh				
1445 vw	*	1446 vw,sh	*						
1440 w	⇓			1440 m	1440 mw	1443 w,+	1441 vw	1442 m	ν_8(SG)
					1436 mw,sh				
					1419 mw,sh				
1421 m		1421 m		1418 s	1417 s	1420 m	1417 m	*	ν_9(GG)
1415 vw		~1415 w,sh	*	1408 m,sh	1407 mw,sh	1410 w,sh,+	1410 w,sh	1414 m	ν_9(SG)
1409 vw	*								
								1377 vw	
				1371 w					
		1353 vw	⇑						
1348 w	↓,*	1349 vw	*	~1350 vw,sh					
1346 m,+	↑,⇓				1347 m	1343 w	1341 w	1342 m	ν_{10}(SG)
		1335 mw	⇑						
1333 m	↑,⇑	1333 mw	⇓	1345 s	1338 m	1338 w	1338 w	*	ν_{10}(GG)
1327 vw,sh	↓,*								
1324 w,sh	↓,*			1325 s	1328 w,sh	~1325 w,sh			ν_{10}(GG′)
1322 w,+	*								SA or GA fund.
1316 vw,+	*								SA or GA fund.
1302 vw	↑,⇑	1299 vw							ν_{11}(GG)
1300 vw	↓,*								ν_{11}(GG′)
1295 vvw									
1285 vw,sh									
1281 w	↑,⇓	1285 vw	*	1293 s,sh	1297 m,sh	1291 s	1289 s	1288 s	ν_{11}(SG)
1279 vw									
1277 m,+	↓,⇓	1278 vw	*	1275 s,sh	1280 s			1280 m	ν_{12}(SG)
1270 w,+	*	1271 w	*						
1266 vw,sh	*								

TABLE 3 (continued)

Infrared						Raman			Interpretation
Ar matrix		N_2 matrix		Solution 300 K	Amorphous solid 80 K	Liquid 260 K	Amorphous solid 80 K	Crystalline solid 80 K	
600 K[b]	Ann.	600 K	Ann.						
1257 vs	⇓	1256 s	⇓		1260 s,sh				
1251 s	⇑	1250 vs	⇑	1250 vs	1251 vs	1251 w	1249 mw	*	ν_{12}(GG)
1247 m,sh									
1241 m,sh	↓,*	1243 w	*						ν_{12}(GG′)
1238 vw,sh									
1235 vw		1235 vw	⇓						
1231 w,+	↓,*	1231 vw	*						ν_{13}(GG′)
1224 w	⇓	1223 w	⇓						
1222 w	⇓	1221 w	⇑		1221 m,sh	1221 m	1221 m	1217 m	ν_{13}(SG)
1219 w	⇑	1218 w	⇓						
1217 w	*	1216 w	*						
1212 s	⇑	1211 s	⇑	1215 s	1212 s		1212 m	*	ν_{13}(GG)
1209 m,sh	⇑	1206 w,sh							
1148 vvw					1143 vw				
1137 vvw									
1133 vw		1133 vw		1133 w	1131 w	1131 vw	1132 vw	*	ν_{14}(GG)
1128 w		1128 w			1126 vw,sh	1122 vvw,sh	~1120 vvw,sh		
						1108 vvw,sh			
1085 vvw	*				1083 w	1081 vw,sh,+	1083 vvw	*	GG′, SA or GA fund.
1062 vvw	⇓			1065 w	1065 w	1069 vw	1067 vw	1067 m	ν_{14}(SG)
1005 vw,sh	⇓	1009 vw,sh							
1003m	⇓				~1005 s,sh			1009 w	ν_{15}(SG)
999 s	↑,⇑	999 s	⇑	991 vs	997 vs	996 vw	1000 vw	*	ν_{15}(GG)
994 m	↑,⇑	995 m,sh	⇓						
970 mw	↑,⇑	970 mw		966 m	969 m	968 vw	970 vw	978 vw	ν_{16}(SG),ν_{16}(GG)
955 vvw									ν_{13}(SA)?
948 vw	*								ν_{22}(SA)?
936 s,sh,+	↓,*	940 s	⇑						

934 vs	↑,⇑	935 s	⇓	933 vs	940 w	940 w	946 w	*	ν_{17}(GG)
928 w,+	*								ν_{17}(GA)
924 m,sh,+	⇓					932 w	932 w	934 w	ν_{17}(SG)
922 m,sh,+	↓,*								ν_{17}(GG′)
920 s	↑,⇑	921 s		925 s,sh	921 s	921 vw,sh	922 w	917 w	ν_{18}(SG), ν_{18}(GG)
					~900 vw	899 vw,sh,+	902 vw	*	GG′, SA or GA fund.
887 s	↑,⇑	885 s	⇓						
885 s,sh									
882 m,sh		881 s	⇑	875 s	875 vs	874 s	874 s	*	ν_{19}(GG)
879 w,sh									
873 w,+	↓,*	874 vw	*						ν_{19}(GG′)
856 vvw					857 w,sh	857 m,sh,+	856 w	856 m	ν_{19}(SG)
719 w,sh	↓,*								ν_{20}(GG′)
717 w,sh									
712 m	↑,⇑	708 m	⇑	706 s	708 s	~706 w	711 w	*	ν_{20}(GG)
709 m,sh	↑,⇑								
704 w,sh	↑,⇑	702 m	⇓						
698 vw,sh									
690 vw,sh,+	⇓								
688 vw,sh,+	⇓				~695 m,sh	~685 vw,sh,+	~690 vw,sh	688 w	ν_{20}(SG)
657 vw,+	*			~660 w	662 vw	663 vw,+	~660 vvw		ν_{20}(GA)
624 vvw,+	*				625 w	~630 vw,sh,+			ν_{20}(SA)
611 vw,	↑,⇑	610 w	⇑						
608 vw,	↑,⇑	608 vw	⇑	603 m	608 m	608 m	610 m	*	ν_{21}(GG)
606 vw,sh+									ν_{21}(GA)
597 vw,+	*				598 vw,sh	~600 w,sh			ν_{21}(GG′)
570 vvw							~570 vw,sh	570 vw	ν_{21}(SG)
567 w,sh	⇓								
565 m	↑,⇑	564 m		558 s	562 s	564 w	565 w		ν_{22}(GG)
559 vw,+	⇓	560 vw	*					564 w	ν_{22}(SG)
556 w,+	*								SA or GA fund.
554 w,+	↓,*			~550 m,sh	554 m,sh		~555 vw,sh		ν_{22}(GG′)

TABLE 3 (continued)

Infrared						Raman			Interpretation
Ar matrix		N_2 matrix		Solution 300 K	Amorphous solid 80 K	Liquid 260 K	Amorphous solid 80 K	Crystalline solid 80 K	
600 K[b]	Ann.	600 K	Ann.						
552 vw,+	⇓				540 vw	543 vw	543 vw	543 w	ν_{23}(SG)
					425 w,br	420 m	424 m	*	ν_{23}(GG)
~360 vvw,sh	*								ν_{23}(GA)?
354 mw	↑,⇑	352 mw			355 m,br	355 w	360 w	*	ν_{24}(GG)
		349 mw	*	344 m					
359 w,+	*				340 vw	343 w,+	~345 vw	*	ν_{24}(GA)
355 vw,+	↓,*								ν_{24}(GG′)
~295 vvw				293 w	~295 w,br	290 w,+	293 w	295 m	ν_{24}(SG)
~275 vvw				278 vw	277 w,br	276 w,+	281 w	*	ν_{17}(SA)?
232 vw	⇑	230 vw							ν_{25}(GG)
				225 m	228 m,br	223 m	230 m	262 m	ν_{25}(SG)
226 vw,+	⇓	224 w							
						~160 w	~170 mw,sh	175 m	ν_{26}(SG)
								123 m	
					~100 w,br			96 s	
							~75 s,br	75 vs	
								51 w	
								37 m	

[a]Weak bands in the regions 4000–3150, 2850–2150 and 2000–1700 cm^{-1} have been omitted.

[b]Temperature of the gas before deposition upon the cold window.

[c]Abbreviations: s, strong; m, medium; w, weak; v, very; br, broad; sh, shoulder; ↓ and ↑ denote bands which decrease or increase in relative intensity upon annealing at 27 K; ⇓ and ⇑ denote bands which decrease or increase in relative intensity upon annealing at 35 K; + denote bands which increase in relative intensity with increasing (nozzle) temperature and * denotes bands which disappear upon annealing.

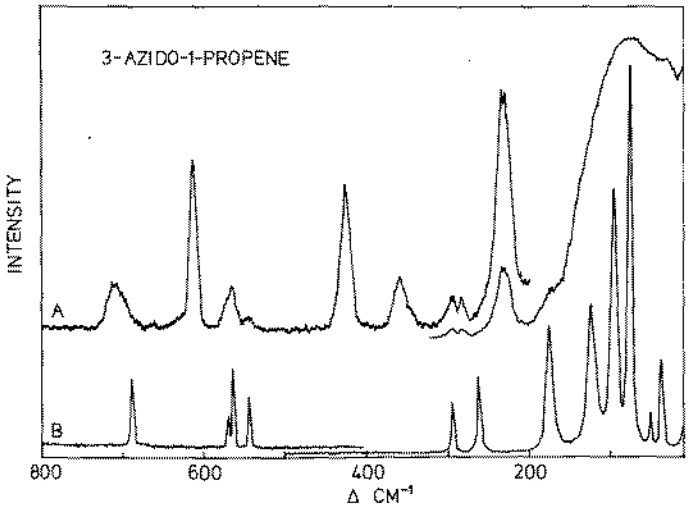

Fig. 2. Raman spectra (800–10 cm^{-1}) of solid 3-azidopropene. (A) Amorphous solid at ca. 80 K. (B) Polycrystalline solid at 115 K.

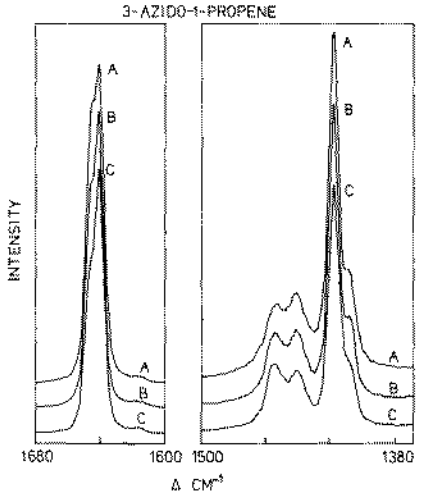

Fig. 3. Raman spectra (1680–1600 and 1500–1370 cm^{-1}) of liquid 3-azidopropene. (A) 248 K, (B) 196 K, (C) 148 K.

Vibrational spectra

The spectroscopic results are listed in Table 3. The Raman lines of the crystalline solid at 37, 262 and 564 cm^{-1}, situated close to the plasma lines of the Ar^+ laser, originate from the sample and not from the Ar^+ laser plasma. In addition to the new IR matrix isolation spectra, a few new very weak bands in

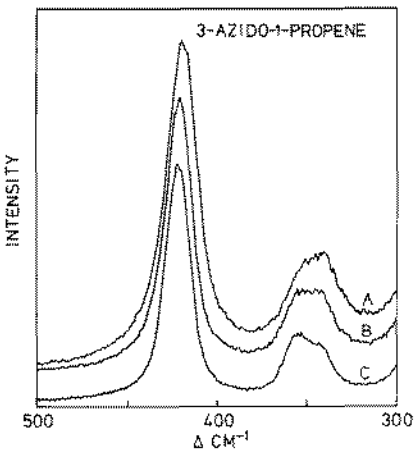

Fig. 4. Raman spectra (500–300 cm^{-1}) of liquid 3-azidopropene. (A) 248 K, (B) 196 K, (C) 148 K.

TABLE 4

Raman integrated intensity data and the derived conformational enthalpy differences with 3σ uncertainty limits for 3-azidopropene in the liquid phase

Temperature (K)	$\frac{I_{955}}{I_{843}}$	$\frac{I_{608}}{I_{630}}$	$\frac{I_{608}}{I_{663}}$	$\frac{I_{1420}}{I_{1410}}$	$\frac{I_{1455}}{I_{1443}}$	$\frac{I_{1642}}{I_{1646}}$
260	0.40	5.19	4.38	1.49	0.13	
248	0.60	7.99	5.11	1.45	0.20	
230		8.55	5.70	1.55	0.34	
216		10.2	6.64	1.62	0.26	0.31
196	0.88	14.8	8.76	1.66	0.34	0.39
178	1.18	17.0		1.73	0.43	0.45
148	1.67			1.98	0.64	0.63
$\Delta H°_{(liq.)}$	3.8(16)	5.2(22)	4.4(7)	1.4(3)	1.3(5)	1.24(16)
Conformer	GG′ + GA	SA	GA	SG	SG	SG

the IR and Raman spectra of the condensed phases have been detected since our previous communication on ALAZ [2].

Raman spectra (800–10 cm^{-1}) of the amorphous and crystalline solids are compared in Fig. 2, and reveal that a number of bands which are present in the spectra of the liquid and the amorphous solid disappear from the crystal spectra. These bands have been marked by asterisks in Table 3. In Figs. 3 and 4 the temperature dependence of selected bands in the Raman spectrum of liquid

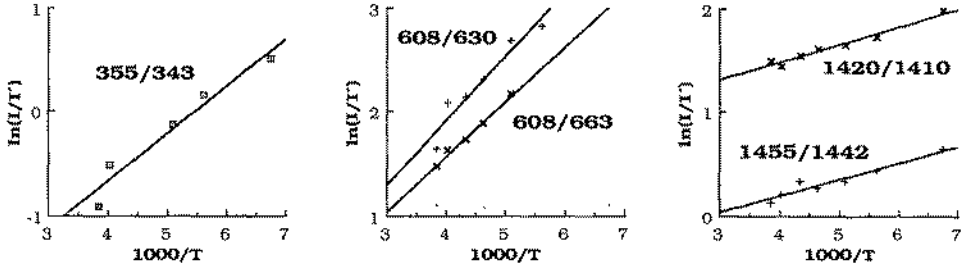

Fig. 5. Van 't Hoff plot of five band pairs of ALAZ as a liquid measured by Raman spectroscopy.

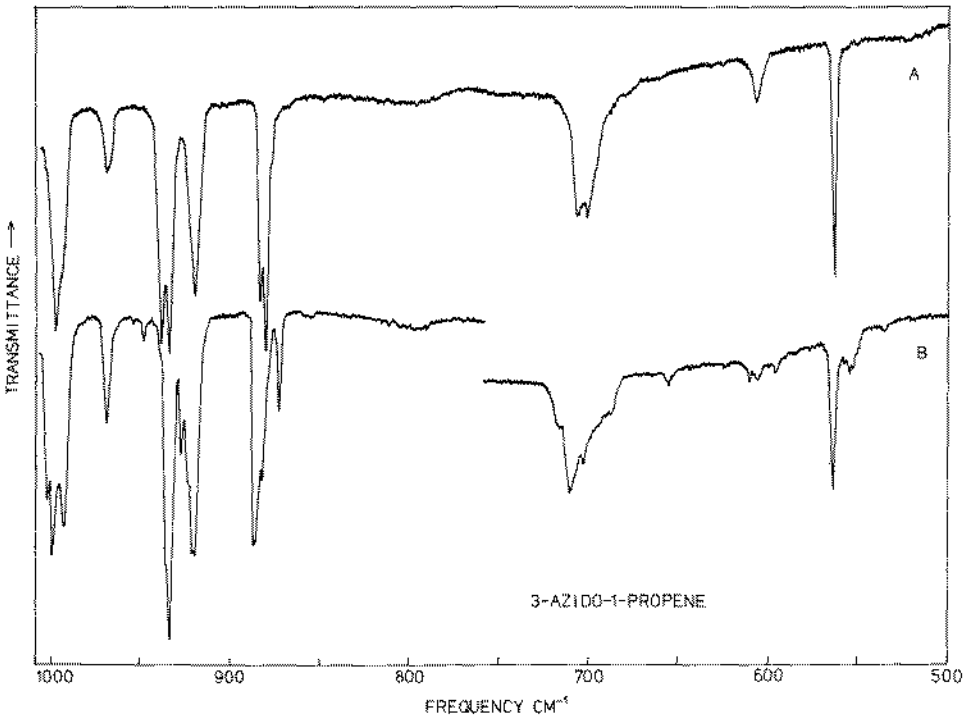

Fig. 6. IR matrix isolation spectra (1000–500 cm^{-1}) of 3-azidopropene, M/A ≈ 1/700, nozzle temperature 600 K. (A) N_2 matrix, (B) Ar matrix.

ALAZ are shown. The Raman bands which clearly increase their relative intensity with increasing temperature have a plus sign in Table 3.

The conformational enthalpy differences between the two most abundant conformers have been determined from Raman temperature spectra of the liquid. Because of frequently overlapping bands and temperature dependence of the band widths, the Raman line intensities were calculated by a least-squares curve-fitting procedure, assuming Lorentzian band shapes. Table 4 summa-

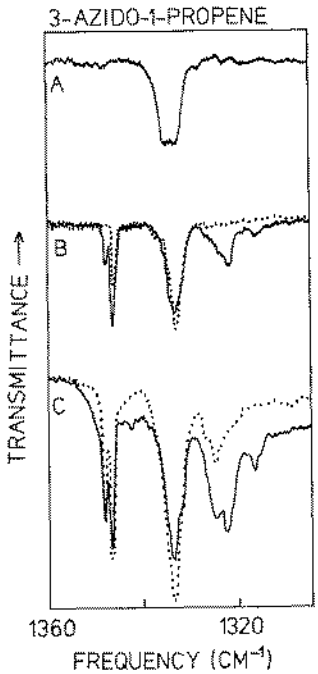

Fig. 7. IR matrix isolation spectra (1360–1300 cm^{-1}) of 3-azidopropene, M/A ≈ 1/700. (A) N_2 matrix, nozzle temperature 300 K; (B) Ar matrix, nozzle temperature 300 K, dotted curve after annealing 35 min at 30 K; (C) Ar matrix, nozzle temperature 450 K, dotted curve after annealing 30 min at 27 K.

rizes the results from the analysis, and Fig. 5 shows the Van 't Hoff plots of the band pairs at 355/343, 608/630, 608/663, 1420/1410 and 1455/1442 cm^{-1}.

A part of the IR matrix isolation spectra (1000–500 cm^{-1}) obtained using the hot nozzle technique is shown in Fig. 6. Both the N_2 and Ar matrix spectra shown were obtained using a nozzle temperature of 600 K. As seen in Fig. 6, the number of bands in the two matrices differs considerably. The variations in the N_2 and Ar matrix spectra are further documented in Fig. 7 (1360–1300 cm^{-1}), which also illustrates the effects of different nozzle temperatures as well as subsequent annealing at different temperatures. The bands which increase in relative intensity with increasing nozzle temperature are marked with a plus sign in Table 3.

The changes in the relative band intensities upon annealing the Ar matrix at 27 K are indicated by single arrows in Table 3, and the subsequent changes after annealing the matrices at 35 K are indicated with double arrows. The bands that disappear from the matrix isolation spectra upon annealing are marked with asterisks.

DISCUSSION

It is obvious from a rapid perusal of the vibrational spectra (Figs. 2–4, 6 and 7) that they have to be interpreted in terms of several conformers being present in the vapour and liquid phases. The question is only: how many are present? To make the discussion of the conformational equilibria intelligible, the theoretical predictions are discussed first and our interpretation of the experimental data is presented later.

Ab initio calculations

We have previously pointed out [5] that the applied double zeta basis set does not provide a near Hartree–Fock limit description of the azide group: the charge distribution is incorrect, the C–N and the central N–N distances are computed to be longer than experimentally observed distances, and the corresponding force constants are too small. Further, the computed gross atomic charge distribution of the azide group is erroneous. Calculations which use large basis sets [5,15,16] show unambiguously that the central N has a positive net charge, contrary to the present results. However, as we are aware of these shortcomings, the calculations do have some merit after all.

If 1–1.5 kJ mol^{-1} is regarded as the lower limit for the reliability of conformational energy differences, calculated at the Hartree–Fock level of approximation, the five conformers can be divided into three groups (see Table 1): (1) GG, (2) SG at ca. 2 kJ mol^{-1} higher energy, and (3) SA, GA and GG′ at further ca. 4 kJ mol^{-1} higher energy. As mentioned in the Introduction, the electron diffraction data could equally well be interpreted in terms of (1) a mixture of two conformers, 73(15)% GG and 27% SG, or (2) a mixture of equal amounts of the GG and GG′ forms, 87(20)% in total, and 13% SG, or (3) a linear combination of these two extremes. The present ab initio calculations (Table 1) agree with the experimental results, which indicates that the SA and GA conformers are present only in very small amounts in the vapour at 300 K. The calculations also support the electron diffraction analysis [2] based upon only the GG and SG forms being present at 300 K. The experimental values for the conformational composition, 73(15)% GG and 27% SG, comply well with the "theoretical" value found in this work. The present calculations rule out the second possible interpretation of the electron diffraction data, i.e. equal amounts of the GG and GG′ forms. However, the calculations do not invalidate the possibility that the GG′ form is present in small amounts, i.e. 5–10%, at 300 K. At higher temperatures (e.g. at 600 K) all five conformers are predicted to be present in amounts which should be easily detectable by IR and Raman spectroscopy.

The most obvious discrepancies between the computed and observed structural parameters are, as mentioned previously, the C–N and the central N–N

distances, which are calculated to be too long, whereas equilibrium distances which are too short are expected in the Hartree–Fock limit. Also, the adjacent angles to these bonds seem to be slightly inaccurate. However, considering the fundamental difference between the two types of structural parameters, the overall agreement is satisfactory. Following the results from a microwave study of 3-fluoropropene [17], the electron diffraction structure refinement [2] supposed the CCC and the CCN angles in ALAZ to be 1.5° larger in the SG form than in the GG form. As seen from Table 2, these assumptions are supported by the results from the present calculations, as is also the bent "transoid" azide group.

Raman spectra

The ab initio calculations show all the conformers of ALAZ to have roughly the same dipole moment. Hence, one would expect only minor changes in the conformational composition on going from the vapour to the liquid phase. At room temperature the liquid should be composed of the GG and SG forms in a roughly 3:1 ratio, whereas the other conformers ought to be present in only small amounts. This is also in agreement with the spectral data, which show no significant change in the conformational composition between the vapour (matrix) and the liquid.

It is apparent from Table 3 that some of the strongest Raman bands of the liquid are missing in the spectrum of the crystalline solid. It can also be seen that only approximately half of the more than 12 liquid-phase Raman bands, increasing in relative intensity with higher temperatures, have a counterpart in the spectrum of the crystalline solid. The first conclusion to be drawn is that at least three conformers can be identified in the liquid. Further, it can be seen from Table 3 that the bands remaining in the Raman spectrum of the crystalline solid often have counterparts in the Ar matrix spectra. These bands also show an increase in relative intensity with increasing vapour temperature before the trapping on the cold window. Hence, the second conclusion to be drawn is that the most stable conformer in the vapour and in the liquid is not the same conformer which is present in the crystalline solid.

It appears reasonable that if the crystal is not composed of the GG then it must consist of the SG conformer. This is confirmed by the temperature dependence of the Raman spectra as well as by the observed changes in the IR matrix isolation spectra with changing nozzle temperature (see below).

Some of the Raman bands show an "irregular" intensity variation with temperature, which may be explained by the bands originating from several conformers. This is a general problem encountered in the calculation of enthalpy differences from band intensity variations. In the present case, the Raman spectrum is weak and low laser power had to be used. Only a few band pairs suitable for calculating the conformational enthalpy differences in the liquid

phase were observed and even these examples (Table 4 and Fig. 5) are not particularly good.

Obviously, some of the bands used for calculating the conformational enthalpy differences must have contributions from more than one conformer. This is particularly true for the CH_2 deformation and C=C stretching regions where the GG/SG band pairs are found. A simple model calculation in which either a GG or SG band coincides with an SA, GG′, or GA band with the same transition moment reveal that (1) the overlapping will never be detected from Van 't Hoff plots over limited temperature intervals; and (2) the slope of the Van 't Hoff plots will deviate from the correct ΔH° by less than 0.2 kJ mol^{-1}.

As seen from Table 4, the three band pairs at 1420/1410, 1455/1443 and 1642/1646 cm^{-1} give a consistent value $\Delta H^\circ_{GG\rightarrow SG} = 1.3(3)$ kJ mol^{-1}. The results for the other three conformations are more uncertain because only one band pair has been used in each case. The band pair at 355/343 cm^{-1} deserves a special comment, as the 343 cm^{-1} band undoubtedly originates from the GG′ as well as the GA conformer (see Table 3). The normal modes in question are the "same" for the two conformers, mainly a bending of the C=C–C skeleton (see also Table 5 in ref. 2). Assuming the same transition moment for these vibrations in the two conformations and $\Delta H^\circ_{GG\rightarrow GA} = 4.4$ kJ mol^{-1} as derived in Table 4, the slope of 3.8 kJ mol^{-1} in the Van 't Hoff plot will, after correction, correspond to $\Delta H^\circ_{GG\rightarrow GG'} = 3.5$ kJ mol^{-1}.

Although the conformational enthalpy differences in the liquid phase have not been accurately determined, they all appear to be smaller than the hypothetical ab initio values. If the same values are taken as reference, it also appears that the straight-chain SA form has the smallest change in conformational enthalpy between the vapour and the liquid.

IR matrix isolation spectra

A rapid perusal of Table 3 and of Figs. 6 and 7 shows significant differences between the spectra of ALAZ isolated in N_2 and Ar matrices. There are three important points to be noted:

(1) more bands appear in the Ar than in the N_2 matrices,

(2) Fig. 7 reveals a strong variation of the relative band intensities in the Ar matrices with the gas mixture temperature before its deposition on the cold window (14 K) (this is in sharp contrast to the N_2 matrix spectra, which shows hardly any variation with the nozzle temperature),

(3) significant differences between groups of bands appear upon annealing of the Ar matrices (thus, by annealing the Ar matrix for 30 min at 35 K, more than 20 bands disappear completely (group A), and more than 10 other bands decrease in their relative intensity (group B)).

Annealing experiments carried out at 27 K reveal that the group B bands do not change intensity after 30 min. Furthermore, among the group A bands

approximately half disappear rapidly on annealing at 27 K, whereas the remaining bands of group A only decrease slowly in intensity. Some of these spectral changes could be explained by different trapping sites, but it would be difficult, if not impossible, to account for all the observations in this way. As already described, the situation for the N_2 matrix spectra is much simpler. Although a few bands disappear from the spectra upon annealing, the N_2 matrix spectra resemble those of the annealed Ar matrix.

It therefore seems obvious that at least four different conformers are trapped in the Ar matrix when the 600 K hot vapour is condensed on the cold window at 14 K. It is more difficult to decide whether three or only two conformers are trapped in the N_2 matrix under similar conditions. It is equally obvious that the differences in the spectra of the Ar and N_2 matrices have to be explained by different barrier heights to rotational interconversion between the conformers in the two matrices. Similar differences between the barrier heights to internal rotation in Ar and N_2 matrices have been observed for the related compounds allyl alcohol and allyl amine [18] as well as for ethylazide [3]. However, in these three examples the barriers were higher in the N_2 than in the Ar matrix, in contrast to what must be the situation in the present case.

In a very naive scheme for unconcerted rotational interconversion, the barrier heights may be estimated from our ab initio studies on azides reported previously [5,6]. They indicate that the barrier to rotation around the C–N bond is low (i.e. less than 6 kJ mol^{-1}) when eclipsing a C–H bond and of medium height (i.e. 8–10 kJ mol^{-1}) when eclipsing a C–C bond. Further, the barriers to rotation around the C–C bond in ALAZ can be estimated from the spectroscopic results for the 3-fluoro propene [19], 3-bromo propene [20] and for allylamine [21]. Hence, the barrier between the GA and GG′ forms is expected to be low, similar to the barriers from the GA to the GG form and from the SA to the SG form. With the azido group oriented *anti* around the C–N bond, the barrier between the GA and SA minima is judged to be of medium height. Finally, if the orientation around the C–N bond is *gauche*, somewhat higher barriers caused by the additional steric effects are expected, i.e. a barrier of medium magnitude on going from GG′ to GG and of medium to high value on going from SG to GG.

If the suggested scheme is valid, one would expect a maximum of three conformers present in the matrices formed at 14 K. Remembering the sequence in conformational energy (SA, GA, GG′ > SG > GG), the GA conformer would convert during deposition to either the GG′ or the GG forms and correspondingly the SA conformer would convert into the SG form. If the energy difference between the GA and the GG′ conformers is not too large, the GG′ conformer would convert through the GA and eventually into the GG form. Thus, the GG, SG and possibly also the GG′ form can be expected to survive the deposition phase of the matrix isolation experiment as carried out here. This simple picture seems to describe the situation in the N_2 matrix experiments.

The bands which disappear from the N_2 matrix spectra upon annealing are then predicted to be either SG bands or GG′ bands.

The same model can be applied successfully to the Ar matrix experiments if we assume that either the barriers for some unknown reason are slightly higher here than in the N_2 matrix or the cooling is more efficient and the trapping time shorter with Ar as the matrix gas. The bands which disappear rapidly upon annealing at 27 K must have their origin in the SA or GA conformer; the bands which disappear more slowly must be due to the GG′ form and, finally, the bands which decrease in intensity only after annealing for 30 min at 35 K must correspond to the SG form. This model explains why our attempts to estimate barrier heights from the annealing experiments were futile. It also explains why reliable information on conformational energy differences could not be obtained from the hot nozzle experiments; this was because of rotational interconversion during the deposition.

The vibrational assignments proposed in Table 3 not only comply with the naive scheme for rotational interconversion but also with our previously calculated normal modes of vibration for the five conformations of ALAZ (see Table 5 in ref. 2).

Our results from relative band intensity measurements as a function of the ALAZ–Ar gas mixture temperature before deposition on the cold window are too embarrassing to print here. The results vary with the deposition speed and, of course, with the temperature of the cold window. Obviously, our equipment is not good enough for such demanding measurements. In spite of this we dare to give the average results (without uncertainties or comments) from several band pairs: $\Delta H^{\circ}_{GG\rightarrow SG} = 1.5$ kJ mol^{-1}, $\Delta H^{\circ}_{GG\rightarrow GG'} = 2.9$ kJ mol^{-1} and $\Delta H^{\circ}_{GG\rightarrow GA} = 44$ kJ mol^{-1}.

ACKNOWLEDGEMENTS

The authors are grateful to Anne Horn for drawing the figures. A.G. acknowledges a postdoctoral fellowship from the Royal Norwegian Council for Scientific and Industrial Research.

REFERENCES

1 P. Klaeboe and C.J. Nielsen, in R. Salzer, H. Kriegsmann and G. Werner (Eds.), Proc. Analytiktreffen 1988, 125, Teubner-Texte zur Physik, Leipzig, 1988.
2 P. Klaeboe, K. Kosa, C.J. Nielsen, H. Priebe and S.H. Schei, J. Mol. Struct., 176 (1988) 107.
3 C.J. Nielsen, K. Kosa, H. Priebe and C.E. Sjøgren, Spectrochim. Acta, Part A, 44 (1988) 409.
4 C.E. Blom and C. Altona, Mol. Phys., 3 (1977) 875.
5 C.J. Nielsen and C.E. Sjøgren, J. Mol. Struct. (Theochem), 150 (1987) 361.
6 J. Almlöf, G.O. Braathen, P. Klaeboe, C.J. Nielsen, H. Priebe and S.H. Schei, J. Mol. Struct., 160 (1987) 1.

7 Hs. H. Günthard, J. Mol. Struct., 80 (1982) 87.
8 F.A. Miller and B.M. Harney, Appl. Spectrosc., 28 (1968) 350.
9 J. Almlöf, MOLECULE, Program manual, USIP Report 74-16, University of Stockholm, 1974.
10 S. Sæbø, MOLFORC, Program manual, University of Oslo, 1980.
11 B. Roos and P. Siegbahn, Theor. Chim. Acta, 17 (1970) 209.
12 S. Huzinaga, J. Chem. Phys., 53 (1965) 1293.
13 T.H. Dunning, Jr. J. Chem. Phys., 55 (1971) 716.
14 E.A. Schott-L'Vova and Ya.K. Syrkin, Izvest. Akad. Nauk SSSR, Ser. Fiz., 14 (1952) 478.
15 A. Sevin, J.P. Leroux, B. Bigot and A. Devarquet, Chem. Phys., 45 (1980) 305.
16 E. Kosmus, E. Nachbaur and K. Faegri, Jr., J. Chem. Soc., Faraday Trans. 2, 72 (1976) 802.
17 E. Hirota, J. Chem. Phys., 42 (1965) 2071.
18 B. Silvi, F. Froment, J. Corset and J.P. Perchard, Chem. Phys. Lett., 18 (1973) 561.
19 J.R. Durig, T.J. Geyer, T.S. Little and D.T. Durig, J. Mol. Struct., 172 (1988) 165.
20 J.R. Durig and M.R. Jalilian, J. Phys. Chem., 84 (1980) 3543.
21 J.R. Durig, J.F. Sullivan and C.M. Whang, Spectrochim. Acta, Part A, 41 (1985) 129.